Journal of Rock Mechanics and Geotechnical Engineering

Journal online: www.rockgeotech.org

Strength reduction and step-loading finite element approaches in geotechnical engineering

Yingren Zheng[1, 2*], Xiaosong Tang[1, 2], Shangyi Zhao[1, 2], Chujian Deng[1, 2], Wenjie Lei[3]

[1] *Department of Civil Engineering, Logistical Engineering University, Chongqing, 400041, China*

[2] *Chongqing Engineering and Technology Research Center of Geological Hazard Prevention and Treatment, Chongqing, 400041, China*

[3] *School of Safety Science and Engineering, Henan Polytechnic University, Jiaozuo, 454000, China*

Received 12 January 2009; received in revised form 10 April 2009; accepted 26 May 2009

Abstract: The finite element limit analysis method has the advantages of both numerical and traditional limit equilibrium techniques and it is particularly useful to geotechnical engineering. This method has been developed in China, following well-accepted international procedures, to enhance understanding of stability issues in a number of geotechnical settings. Great advancements have been made in basic theory, the improvement of computational precision, and the broadening of practical applications. This paper presents the results of research on (1) the efficient design of embedded anti-slide piles, (2) the stability analysis of reservoir slopes with strength reduction theory, and (3) the determination of the ultimate bearing capacity of foundations using step-loading FEM (overloading). These three applications are evidence of the design improvements and benefits made possible in geotechnical engineering by finite element modeling.

Key words: finite element limit analysis method; strength reduction; step-loading; embedded anti-slide piles; reservoir slope; foundation

1 Introduction

In 1975, Zienkiewicz [1] proposed that the factor of safety and the limit load used in geotechnical engineering applications could be modeled by increasing the external load or reducing the strength through a finite element method (FEM). In the 1980s and 1990s, FEM was used to analyze the stability of slopes and foundations [2]. However, the lack of a reliable finite element program and an incomplete understanding of strength criteria and handling techniques resulted in inaccuracy in the finite element calculation. As a result, FEM was not widely accepted in geotechnical engineering field.

Several papers [3–6] were published in the late 1990s about the calculated factor of safety for homogeneous soil slopes using a strength reduction FEM. As some of these published results were close to those obtained by traditional methods, the acceptance of the strength reduction FEM increased. The application of this technique ushered in a new era in slope stability analysis. The characterizations of sliding surfaces and calculation of slope factors of safety using strength reduction FEM, and the determination of the ultimate bearing capacity of foundations through step-loading FEM, have now become common practice. The strength reduction theory is now mature, but extensive research on the step-loading technique is still needed. In this paper, these two methods are both called finite element limit analysis methods, because they both adopt the limit analysis concept in their numerical procedures.

In China, Song [7] introduced the study of strength reduction FEM and its application to soil slope stability. Theoretical and applied researches [8–15] have continued with improved accuracy. Some of our earlier works [8, 14–18] advanced the basic theory of strength reduction FEM and played a leading role in its application to the design of anti-slide piles. That earlier works also involved intensive study of the ultimate bearing capacity of foundations by step-loading FEM and its applications [19–21]. This paper summarizes some of our recent progress in these areas.

2 Theory of strength reduction FEM

2.1 Basic theory

At present, the limit state design method is widely

Doi: 10.3724/SP.J.1235.2009.00021

*Corresponding author. Tel: +86-13320267925; E-mail: hnm97@163.com

Supported by the National Natural Science Foundation of China (40318002)

used in geotechnical engineering. Two methods of limit state are commonly used for the analysis of foundation and slope. One is to increase the external load until a critical (limit) state of failure is reached, as in the determination of ultimate bearing capacities for foundations. The other is to reduce the strengths of rock and soil progressively until a critical failure limit state is reached, as in the calculation of the factor of safety for slopes. The specific equation for the factor of safety under limit states varies due to the differences in the adopted limit state methods. As far as the slope is concerned, it is suitable to determine the factor of safety by reducing strength until the failure limit state is reached. This is the factor of safety of the strength reserve that is widely used in slope stability analysis. The strength reduction method using FEM can be used to simulate the failure limit states of slopes and thus to determine their sliding surfaces and factors of safety.

Strength reduction means reducing the parameters of shear strength (cohesion and internal friction angle) of soil (or rock) slopes in the finite element calculation, within a theoretical framework of perfect elastoplasticity, until the limit failure state is reached. Then, the sliding surface of the slope can be automatically obtained from the results of the elastoplastic FEM, and the factor of safety of strength reserve can be calculated.

The factor of safety of the strength reduction method can be expressed as follows:

$$\omega = \tau / \tau' \tag{1}$$

where τ is the initial shear strength of geotechnical materials, and τ' is the shear strength under limit state after reduction.

Different yield criteria can be adopted in strength reduction FEM. The expression of τ varies according to its yield criterion. Taking the Mohr-Coulomb yield criterion (shown in Fig.1) for instance, $\tau = c + \sigma \tan\varphi$, and its strength reduction process is described by

$$\tau' = \frac{\tau}{\omega} = \frac{c + \sigma\tan\varphi}{\omega} = \frac{c}{\omega} + \sigma\frac{\tan\varphi}{\omega} = c' + \sigma\tan\varphi' \tag{2}$$

$$\left.\begin{aligned} c' &= \frac{c}{\omega} \\ \tan\varphi' &= \frac{\tan\varphi}{\omega} \end{aligned}\right\} \tag{3}$$

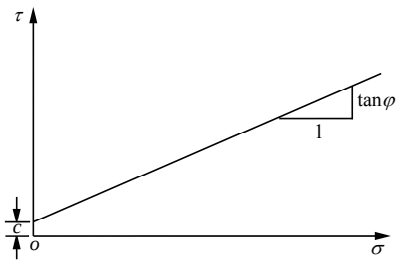

Fig.1 Mohr-Coulomb yield criterion.

Therefore, the strength reduction is identical to the way of defining the factor of safety in traditional limit balance slice methods for slope stability analysis. In the traditional limit balance slice methods, a sliding surface is assumed first and then the factor of safety is calculated according to the equilibria of forces and/or moments. Then, the factor of safety ω is defined as the ratio of anti-slide forces (or moments) to sliding forces (or moments) along the sliding surfaces:

$$\omega = \frac{\int \tau_{\mathrm{L}}\,\mathrm{d}l}{\int \tau_{\mathrm{s}}\,\mathrm{d}l} = \frac{\int_0^l (c + \sigma\tan\varphi)\mathrm{d}l}{\int_0^l \mathrm{d}l} \tag{4}$$

where τ_{L} is the local shear strength at each point on the sliding surface, l is the length of the bottom edge of soil slice, and τ_{s} is the actual local shear stress at each point on the sliding surface. Dividing the above equation by ω on both sides, the following expression can be obtained:

$$1 = \frac{\int_0^l \left(\frac{c}{\omega} + \sigma\frac{\tan\varphi}{\omega}\right)\mathrm{d}l}{\int_0^l \tau_{\mathrm{s}}\,\mathrm{d}l} = \frac{\int_0^l (c' + \sigma\tan\varphi')\mathrm{d}l}{\int_0^l \tau_{\mathrm{s}}\,\mathrm{d}l} \tag{5}$$

Apparently, in traditional limit balance methods, the indexes of shear strength c and $\tan\varphi'$ are reduced to c/ω and $(\tan\varphi)/\omega$ under limit state (the factor of safety is 1), respectively. The parameter ω is now called the factor of safety, which is equivalent to the strength reduction factor.

2.2 Constitutive relations and yield criteria for the finite element limit analysis method

As the stability analysis is related to the analysis of force and strength instead of displacement, a perfect elastoplastic constitutive model is sufficient for accurate finite element calculations without the consideration of hardening and softening rocks or soils [8]. The yield criterion is very important in the finite element limit analysis method as it has great effects on the computational results. The Mohr-Coulomb yield criterion is often adopted in practical geotechnical engineering and its expression is

$$\sigma_1(1+\sin\varphi) - \sigma_3(1-\sin\varphi) = 2c\cos\varphi \tag{6}$$

or

$$\frac{I_1\sin\varphi}{3} + \cos\theta_\sigma - 3^{1/2}\sin\theta_\sigma\sin\varphi_2^{1/2} = c\cos\varphi \tag{7}$$

where I_1 is the first invariant of the stress tensor.

The Mohr-Coulomb yield surface on the π-plane is an irregular hexagon (shown in Fig.2) that introduces a numerical difficulty into the finite element calculations. Therefore, it is necessary to modify the Mohr-Coulomb yield surface approximately or to adopt the generalized Mises yield criterion that is related to the Mohr-Coulomb yield criterion.

The generalized Mises yield criterion, based on the Mises

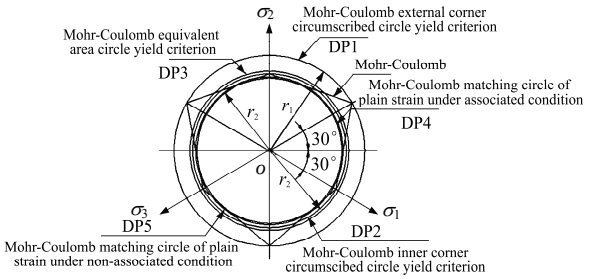

Fig.2 The yield surface on the π-plane.

yield criterion, considers the average compressive stress, and it can be expressed as follows:

$$\left.\begin{aligned} &\alpha I_1 + J_2^{1/2} = k \\ &I_1 = \sigma_1 + \sigma_2 + \sigma_3 \\ &J_2 = \frac{(\sigma_1-\sigma_2)^2 + (\sigma_1-\sigma_3)^2 + (\sigma_2-\sigma_3)^2}{6} \end{aligned}\right\} \quad (8)$$

where J_2 is the second invariant of the deviator stress tensor, and the material constants α, k are related to the Coulomb's material constants (c or φ) in different ways, as described in Table 1.

Table 1 Relationship of yield criteria.

Yield criteria	α	k
DP1: Mohr-Coulomb criterion based with external corner circumscribed, a circle yield criterion	$\frac{2\sin\varphi}{\sqrt{3}(3-\sin\varphi)}$	$\frac{6c\cos\varphi}{\sqrt{3}(3-\sin\varphi)}$
DP2: Mohr-Coulomb criterion based with inner corner circumscribed, a circle yield criterion	$\frac{2\sin\varphi}{\sqrt{3}(3+\sin\varphi)}$	$\frac{6c\cos\varphi}{\sqrt{3}(3+\sin\varphi)}$
DP3: Mohr-Coulomb criterion based with equivalent area, a circle yield criterion	$\frac{2\sqrt{3}\sin\varphi}{\sqrt{2\sqrt{3}\pi(9-\sin^2\varphi)}}$	$\frac{6\sqrt{3}\cos\varphi}{\sqrt{2\sqrt{3}\pi(9-\sin^2\varphi)}}$
DP4: Mohr-Coulomb crietrion based with matching circles, for plain strain problems with associated flow rules	$\frac{\sin\varphi}{\sqrt{3}\sqrt{3+\sin^2\varphi}}$	$\frac{3c\cos\varphi}{\sqrt{3}\sqrt{3+\sin^2\varphi}}$
DP5: Mohr-Coulomb criterion based with matching circle, for plain strain problems with non-associated flow rules	$\frac{\sin\varphi}{3}$	$c\cos\varphi$

Different values of α and k result in different extended Mises yield criteria with yield surfaces on the deviator plane that trace different circles (Fig.2).

Equation (8) was established by Drucker and Prager in 1952. So, the generalized Mises yield criterion is also called the Drucker-Prager yield criterion. This criterion is visualized as a conical surface in principal stress space. The cross-sectional shape of this cone on the π-plane is a circle, which readily facilitates numerical computations. In the generalized Mises yield criterion, the yield criteria represented by circumscribed circles DP1, DP2 and DP4 are commonly used internationally. We propose new yield criteria DP3 and DP5. The DP3 criterion is suitable for 3D problems, and criterion DP5, like DP4, can be used for 2D plane strain problems.

2.3 Slope failure criteria in strength reduction FEM

When strength reduction based FEM is used to analyze slope stability, one typical problem is how to identify the limit failure state based on the results of finite element calculations. Some methods [9–15] are presented below.

(1) In finite element calculations, slope failure happens at the same time as the non-convergence of the finite element model solutions, that is, the non-convergence of a finite element model solution can be considered to indicate slope failure.

(2) Generalized shear strain or generalized plastic strain from the bottom to the top of a slope can be used to indicate the sign of slope failure.

(3) The indication of slope failure should be the infinite movement of sliding soil. The strain and displacement on the sliding surface mutate and develop infinitely.

A plastic zone extending from the bottom to the top surface of a slope does not necessarily indicate slope failure. It is a necessary condition of slope failure but not a sufficient condition. The indication of slope failure is that the sliding mass moves infinitely and the strain or displacement mutates, with the simultaneous occurrence of non-convergence for the static finite element model solution.

3 Application of strength reduction FEM to practical engineering

3.1 Design of embedded anti-slide piles

At present, the imbalanced thrust force method (ITFM) is often adopted in the design of anti-slide piles. Geotechnical engineers have tried to improve traditional calculation methods, but there are still many remaining deficiencies. For the first time, we have utilized a strength reduction based FEM in the design of anti-slide piles and achieved some satisfying results in theory and practice.

The approach can take the pile-soil interaction into consideration, obtain reasonable resistance in front of the pile (by the distribution of thrust and resistance), determine an appropriate length for embedded anti-slide piles, calculate the thrust and resistance imposed on the embedded anti-slide piles, and optimize the composite forms of anti-slide piles such as anchorage piles and bracing piles. An example of strength reduction FEM applied to the design of embedded anti-slide piles is provided below.

3.1.1 *Determination of a reasonable pile length*

The parameters in Table 2 are adopted for the analysis of a typical section of a slope with a landslide body located within a colluvium deposit (shown in Fig.3) at Yuhuangge in the new Wushan County, located in the area of the Three Gorges reservoir. The landslide body, slip zone and an underlying stable rock stratum are represented by domain elements. The embedded anti-slide piles are represented by beam elements. The analysis was conducted to determine the relationships between the pile length, the factor of safety and the sliding surface. The length of the anchorage pile section beneath the slip zone is set to 3 m. Eight piles were designed to sink down into the hill below the road (shown in Fig.3); their lengths are 7, 9, 11, 13, 15, 17, 19 and 21.22 m. If the top of a pile extends to the ground surface, it is called a full-length pile.

Table 2 Physico-mechanical parameters for the analysis of a landslide body at Yuhuangge.

Materials	Unit weight (kN/m^3)	Elastic modulus (MPa)	Poisson's ratio	Cohesion (kPa)	Internal friction angle (°)
Landslide soil	21.4	30	0.3	34	24.5
Slip soil	20.9	30	0.3	24	18.1
Landslide bed	23.7	1.7×10^3	0.3	200	30.0
Pile (C25 concrete)	24.0	29×10^3	0.2	Treated as liner elastic material	

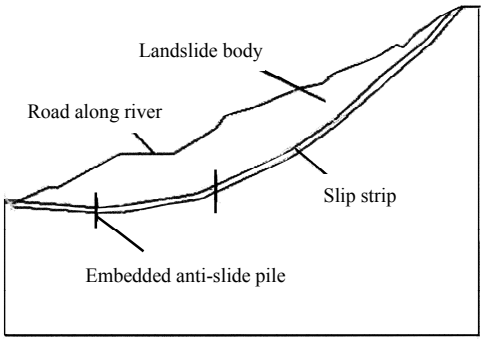

Fig.3 Landslide body, road and anti-slide pile layout over a landslide body at Yuhuangge.

At first, according to the calculated results of strength reduction FEM, the factor of safety of the slope under gravity was determined as 1.02, whereas the factor of safety calculated by conventional limit equilibrium analysis was 1.04.

Several key issues were investigated. These issues with the obtained results and conclusion are discussed below.

(1) *The relation between the pile length and the location of sliding surface*

Positioning the sliding surface is a very important aspect of slope stability studies. Variation in the location of the sliding surface with different pile lengths is shown in Fig.4.

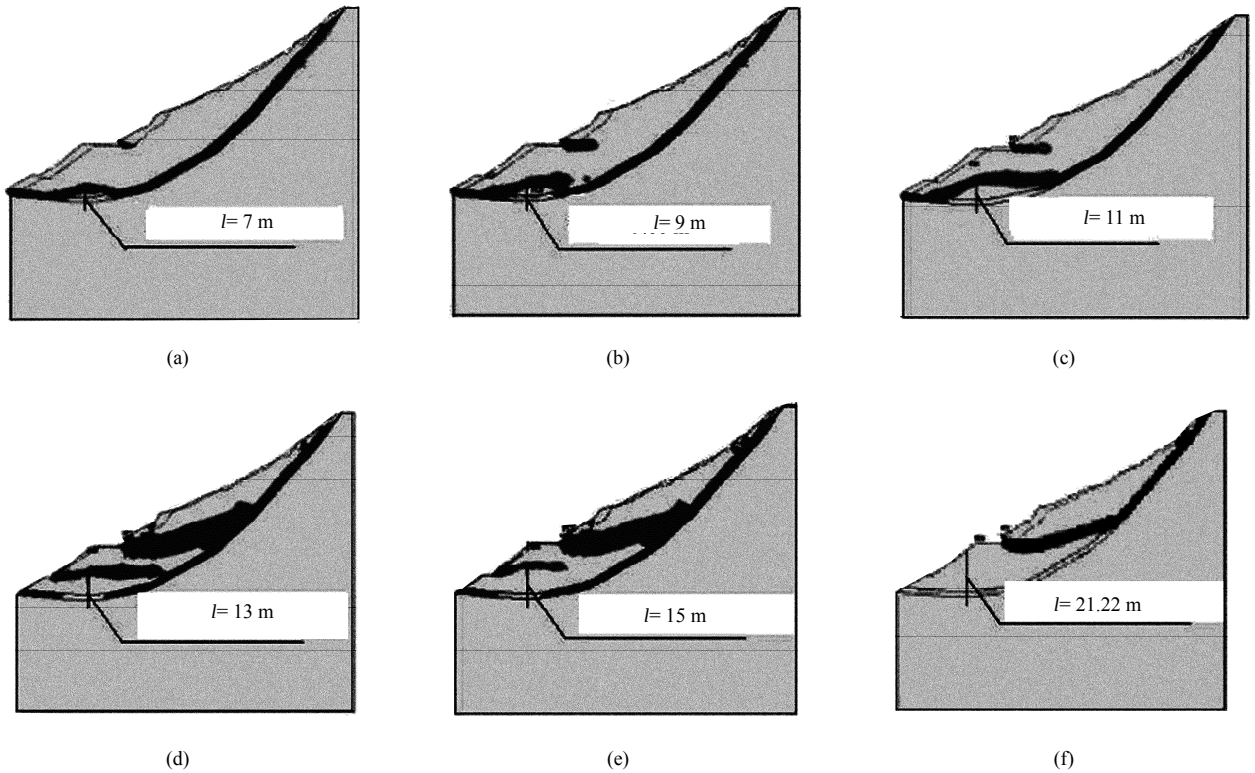

Fig.4 Changes of length and sliding surface positions.

When the embedded pile length was set to 7–11 m and the pile position was below the road, a landslide could take place with the sliding surface slipping over the top of the anti-slide piles (Fig.4). When the pile length was set to 13 m, two sliding surfaces developed. The first one was close to the top of the pile with a new sliding surface outcropping on the downhill face of the road slope, and the other was a secondary sliding surface of a plastic zone exposed in the toe of the road slope. When the pile length was set to 15 m, with the top of the pile still under the ground surface, only the secondary sliding surface appeared at the same location when the pile length was 13 m. The position of the sliding surface remained the same until the full-length (21.22 m) pile was used and the top of the pile reached the slope surface.

(2) *The relationship between pile length and the factor of safety*

The results from the strength reduction finite element model were used to calculate factors of safety with different pile lengths. The results are shown in Table 3.

Table 3 Relationship between pile length and factor of safety when the piles are below the road.

Pile length (m)	Factor of safety	Pile length (m)	Factor of safety
0	1.02	13	1.19
7	1.13	15	1.19
9	1.15	21.22	1.19
11	1.19	—	—

Assuming that the embedded anti-slide piles would not fail under the loading of the slope, then the change of pile length should also change the factor of safety of the slope. The shorter the pile is, the lower the factor of safety is. When the pile is on the downhill side of the road (as shown in Table 3), with the pile length changing from 7 to 11 m in the finite element model, the factor of safety increases from 1.13 to 1.19. The factor of safety remains at 1.19 with the pile lengths of 11, 13, 15 and 21.22 m. It means that increasing the pile length does not enhance the safety of the slope beyond a 13 m length. In this case, however, because the required factor of safety is 1.15, the appropriate pile length should be 9 m, as shown in Table 3.

3.1.2 *The landslide thrust on the anti-slide section of piles*

When calculating the internal forces inside the pile, the thrust behind the pile and the resistance in front of the pile should also be calculated. The thrust can be determined by traditional methods, and the resistance can be set to an assumed approximate value or zero. If beam elements are used to represent anti-slide piles in a finite element model, the strengths of geotechnical materials need to be reduced to their ultimate states so that the thrust and internal force can be obtained directly.

However, the net thrust is the difference between the thrust behind the pile and the resistance in front of the pile. If the resistance behind the pile is zero, the net thrust is equal to the thrust in front of the pile. As a result, the strength reduction FEM should be adopted to calculate the resistance behind the pile, and there should be no soil in front of the pile. The internal forces are usually expressed as moments and shear forces. The values of shear force can be calculated directly without using the thrust first. For the slope stability example presented above, the calculated thrust is shown in Table 4.

Table 4 Landslide thrust when the factor of safety is 1.15.

Pile length (m)	Landslide thrust on the anti-slide section (kN)	The ratio of landslide thrust (compared with that for full-length pile) (%)
9	11 405	70.9
15	15 237	83.4
19	16 167	100.5
21.22	16 085	100.0

The landslide thrust on the anti-slide section of a 9 m embedded pile is 11 405 kN, which is 70.9% of the landslide thrust on a full-length pile; the landslide thrust on a 15 m pile is close to that of the full-length pile, and a pile with length of 19 m will have a thrust that almost equals that of the full-length pile. It is apparent that if the factor of safety remains the same (1.15 in this case), the shorter the pile is, the smaller the thrust is. Therefore, the sliding mass on the top of the pile can bear a part of the landslide thrust, which illustrates the advantage of the embedded anti-slide piles. The idea that embedded piles bear the complete landslide thrust is incorrect.

3.1.3 *The internal forces of embedded anti-slide piles*

When calculating the internal forces through the strength reduction FEM, the internal forces (including shear forces and moments) of embedded anti-slide piles can be also calculated. Table 5 shows the calculated internal forces for the example presented above and its ratio to the maximum values of internal forces for the full-length pile case. The calculated internal forces of embedded anti-slide piles are found to be more reasonable than those of full length piles; the passive shear on the anchoring section of the embedded anti-slide piles (S_{pi}) is lower than that on the full-length pile. The shear force on the anti-slide section (S_{oi}) is a little higher than that on the full-length pile, and the moment of the embedded anti-slide piles (M_i) is lower than that of the full-length pile. When the pile length is 9 m, the factor of safety reaches 1.15, which satisfies

Table 5 Comparison of the extreme value of internal force.

Pile length (m)	The maximum shear force on anti-slide section (MN)	The maximum force on anchoring section (MN)	Moment (10^7N·m)	S_{oi} (%)	S_{pi} (%)	M_i (%)
9	1.95	4.92	1.09	92.7	51.9	48.8
11	2.39	7.03	1.61	105.4	74.2	71.8
13	2.36	8.28	1.92	104.3	87.3	86.0
15	2.33	9.04	2.12	103.4	95.4	94.7
21.22	2.22	9.48	2.24	100.0	100.0	100.0

the stability requirement. At the same time, the maximum shear force at the anti-slide section is 92.7% of that of full length pile; the maximum shear force at the anchoring section and the maximum moment at the anti-slide section are 51.9% and 48.8% of those of the full-length pile, respectively. When the pile length is 11 m, the factor of safety is the same as that of the full-length pile. Then the maximum shear force at the anti-slide section is a little higher than that for the full-length pile; the maximum shear force at the anchoring section is 74.2% of that of the full-length pile and the moment is only 71.8%. So, the advantages of the embedded anti-slide piles are obvious: the internal forces of embedded anti-slide piles are preferred to those of the full-length piles while maintaining the same slope stability.

In practical engineering, construction costs would be reduced dramatically by as much as 50% due to the application of shorter embedded piles (compared with full-length piles). The technical advantages and economic efficiency are complementary. Figure 5 shows the changing process of shear forces along the pile (from the calculation results of the strength reduction FEM). Similar examples include the landslide-controlled outlet of Fengjieliang tunnel on the highway between Fengjie and Yunyang, the landslide-controlled Wulong County, and the landslide-controlled B9 section of the highway between Fengjie and Yunyang in Waduan Village.

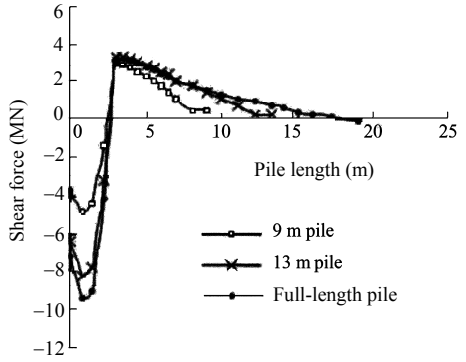

Fig.5 Shear forces changes with pile length.

3.2 Stability of reservoir banks

The problem of slope stability is less complicated when the effects of water are not considered. This assumption, however, cannot often be accepted, especially when considering reservoir banks. Bank stability can be influenced by changing rates of water levels, the permeability of geotechnical materials, and seepage of groundwater. In engineering practice, the locations of phreatic surfaces in reservoir banks are often roughly estimated through empirical generalizations, and the reliability of such estimations needs to be determined. An example is presented below that demonstrates the use of strength reduction finite element models in stability analysis and seepage calculations. This will highlight the sources of inaccuracies that occur when using empirical generalization approaches.

A homogeneous soil slope with a height of 15 m is studied. The unsaturated unit weight of the soil $\gamma_{unsaturated}$ = 17 kN/m^3, the saturated unit weight of the soil $\gamma_{saturated}$ = 18 kN/m^3, the cohesion c = 16.5 kPa, and the internal friction angle φ = 22.6°. The soil coefficients of permeability are 0.1, 0.01 and 0.001 m/d. The line between the water level far from slope and water level after change is generalized as the phreatic surface (Fig.6) if using empirical generalization approaches. In the case, the numerical solution to the phreatic surface location is obtained through the transient fluid flow analysis of the PLAXFLOW seepage module. The slope stability analysis is conducted via the coupling of PLAXIS (for stress analysis) and PLAXFLOW (for seepage analysis) [16–18].

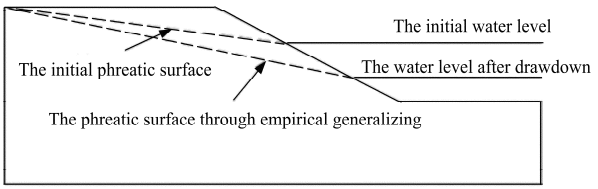

Fig.6 Phreatic surface through empirical generalization.

The hydraulic boundary condition behind the slope is set as a constant water head in this case, h = 35 m. The water level in front of the slope is reduced to a speed of 3 m/d from the initial water level 35 m for 5 days. Water level is therefore reduced by 15 m. The calculation results for the factors of safety are listed in Table 6.

Table 6 Calculated factors of safety.

Water level (m)	Factors of safety			
	Numerical solution by PLAXFLOW seepage module			Results from empirical generalization
	0.1 m/d	0.01 m/d	0.001 m/d	
35	2.119	2.119	2.119	2.119
32	1.705	1.668	1.659	1.832
29	1.424	1.348	1.327	1.622
26	1.262	1.151	1.123	1.495
23	1.197	1.051	1.015	1.441
20	1.225	1.124	1.087	1.447

Note: 0.1, 0.01, 0.001 m/d are permeability, and similarly hereinafter.

Figure 7 shows the sliding surfaces determined numerically through the phreatic surface when the water level is reduced to 23 m and the coefficients of permeability are 0.01 and 0.001 m/d. Figure 8 shows the sliding surface when the empirical generalization of the phreatic surface is used and the water level is reduced to 23 m. Figure 9 shows the relationship between the water level and the factor of safety according to Table 6.

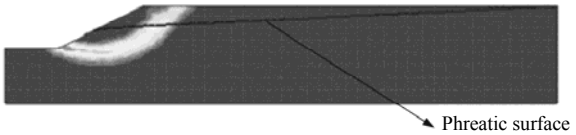

(a) Coefficient of permeability is 0.1 m/d.

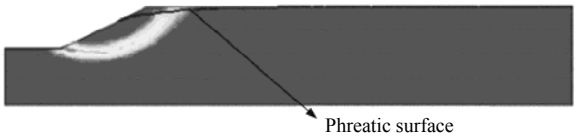

(b) Coefficient of permeability is 0.001 m/d.

Fig.7 Sliding surfaces through the phreatic surface from numerical modeling.

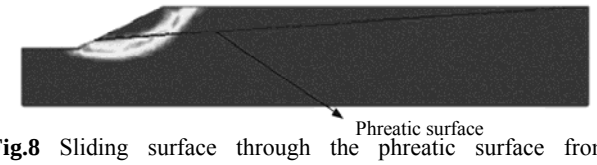

Fig.8 Sliding surface through the phreatic surface from empirical generalization.

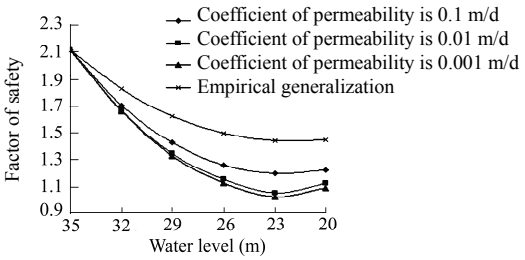

Fig.9 Relationship between water level and factor of safety.

As seen in Table 7, when the water level reaches the same height, the difference with the results from the empirical generalization increases as the coefficient of permeability decreases. When the coefficient of permeability remains constant, the difference of factor of safety increases with the drawdown of the water level.

Table 7 Difference in calculated results of factor of safety.

Water level (m)	Difference		
	Numerical solution by PLAXFLOW seepage module		
	0.1 m/d	0.01 m/d	0.001 m/d
35	0.000 0	0.000 0	0.000 0
32	−0.069 3	−0.089 5	−0.094 4
29	−0.122 1	−0.168 9	−0.181 9
26	−0.155 9	−0.230 1	−0.248 8
23	−0.169 3	−0.270 6	−0.295 6
20	−0.153 4	−0.223 2	−0.248 8

From both the numerical solution and the empirical generalization (Fig.9), it can be observed that the factor of safety reaches its minimum value when the water level is reduced to 23 m. This water level is the most unfavorable water level. So in practical engineering, project design should be based on the corresponding factor of safety of the most unfavorable water level.

In this example, the factor of safety determined by the numerical solution at the most unfavorable water level is 1.197, 0.169 3 lower than the empirically generalized factor of safety. When the coefficient of permeability are 0.01 and 0.001 m/d, the numerical solutions of factor of safety are 0.270 6 and 0.295 6 lower than the empirically determined factor of safety, respectively. Recalling the phreatic surfaces shown in Figs.7 and 8, the main source of the differences in the stability analyses is the different locations of the phreatic surface. The empirically generalized phreatic surface does not take into account the hysteresis effect, so its phreatic surface is lower than those used in the numerical models. The difference increases with a decrease in soil permeability. Therefore, the difference of the calculated results for factor of safety increases as the permeability decreases. As a result, the factor of safety would be overestimated if the phreatic surface is generalized empirically. This would lead to potentially dangerous designs.

4 Finite element limit analysis method for foundation engineering

4.1 Ultimate bearing capacity of rigid and smooth strip foundations when $\gamma = 0$

When the unit weight of the soil $\gamma = 0$, the ultimate bearing capacity of rigid and smooth strip foundations has closed form solutions in Prandtl [22]:

$$q_u = \begin{cases} c\cos\varphi[\exp(\pi\tan\varphi)\tan 2(\pi/4+\varphi/2)-1] & (\varphi \neq 0) \\ (\pi+2)c & (\varphi = 0) \end{cases} \quad (9)$$

A finite element limit analysis model can be used to analyze rigid and smooth strip foundations. The finite element model is shown in Fig.10. The following material constants are used: cohesion c =10 kPa and internal friction angle $\varphi = 0°$–30°. The effect of the dead weight

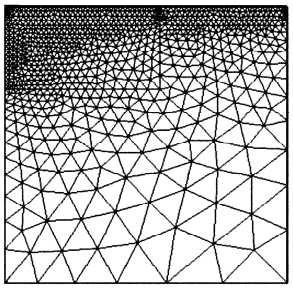

Fig.10 Finite element mesh.

of material is neglected. The yield criterion DP4 is used and an associated flow rule is assumed. The calculated ultimate bearing capacity of the foundations with different internal friction angles is summarized in Table 8.

Table 8 The results of ultimate bearing capacity.

φ (°)	Ultimate bearing capacity (kPa)		Error (%)
	Closed-form solution	FEM	
0	51.42	52.19	1.50
5	64.89	65.96	1.66
10	83.45	84.98	1.83
15	109.77	111.90	1.94
20	148.35	151.75	2.29
25	207.21	212.08	2.35
30	301.40	310.00	2.85

From Table 8, it can be observed that the results of the finite element limit analysis method are very close to the closed-form solution. Almost the same results can be calculated when a non-associated flow rule is applied.

The velocity field under the limit load is shown in Fig.11, and the failure surface at the limit load is shown in Fig.12. The parameters of the failure mechanism obtained from the finite element limit analysis models are shown in Table 9, which are close to the analytical failure mechanism shown in Fig.13 and Table 10.

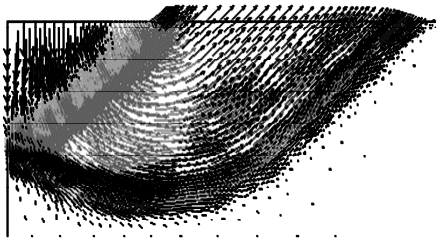

Fig.11 Displacement vector.

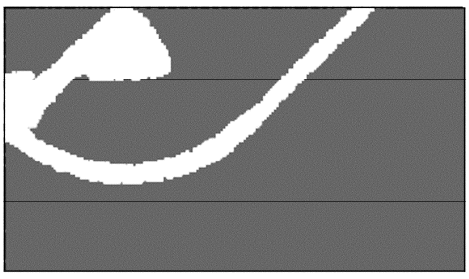

Fig.12 Failure surface under limit state.

Table 9 Some parameters of the analytical failure mechanism.

φ (°)	d_1 (m)	d_2 (m)	h (m)	φ (°)	d_1 (m)	d_2 (m)	h (m)
0	0.50	0.71	1.00	20	0.71	1.16	2.53
5	0.55	0.79	1.25	25	0.79	1.35	3.27
10	0.60	0.89	1.57	30	0.87	1.59	4.29
15	0.65	1.01	1.99	—	—	—	—

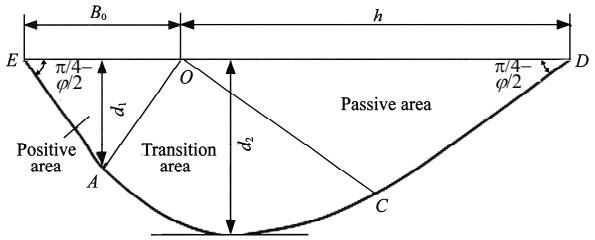

Fig.13 Analytical failure mechanism.

Table 10 Finite element results for the parameters of the analytical failure mechanism.

φ (°)	d_1 (m)	d_2 (m)	h (m)	φ (°)	d_1 (m)	d_2 (m)	h (m)
0	0.49	0.70	0.98	20	0.70	1.19	2.51
5	0.53	0.80	1.25	25	0.75	1.35	3.15
10	0.60	0.90	1.50	30	0.89	1.62	4.20
15	0.65	1.05	1.92	—	—	—	—

The load-displacement curve of the central point of the foundation obtained from the finite element limit analysis method is shown in Fig.14. It can be interpreted that the displacement of the central point of the foundation increases as the load increases, and increases suddenly and sharply when the foundation fails.

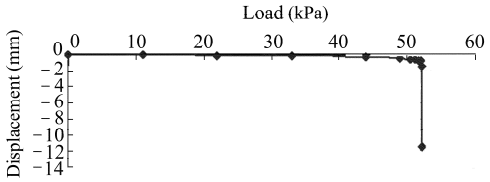

Fig.14 Load-displacement curve of the central point of the foundation during a step-loading process.

4.2 Ultimate bearing capacity of rigid and smooth strip foundation when $\gamma \neq 0$

There are no closed-form solutions for the ultimate bearing capacity of rigid and smooth strip foundation when $\gamma \neq 0$. Some well-known empirical formulas of N_γ have been proposed, such as those presented by Terzaghi, Meyerhof and Vesic [23]. Table 11 shows the finite element results of N_γ compared with empirical estimates. The values of N_γ from the Vesic empirical formula are closest to the finite element values.

Table 11 Values of N_γ from the finite element models and the classical empirical formulas.

φ (°)	N_γ			
	Terzaghi	Meyerhof	Vesic	FEM
5	0.089	0.069	0.449	0.502
10	0.467	0.366	1.224	1.557
15	1.418	1.129	2.647	3.422
20	3.537	2.870	5.386	6.249
25	8.109	6.765	10.876	12.325

4.3 Ultimate bearing capacity of jointed rock foundations

An example of a rock foundation is also analyzed. The properties of the concerned rock are assumed as

follows: cohesion $c_1 = 1.0$ MPa and internal friction angle $\varphi_1 = 40°$. The foundation is intersected by a joint with cohesion $c_2 = 0.1$ MPa and internal friction angle $\varphi_2 = 10°$, and at different inclinations of 25°, 30°, 35°, 40°, 45° or 60° (shown in Fig.15). It is assumed that the width of the rock foundation is *B*. The bearing capacity of the jointed rock foundation can be calculated using the finite element models.

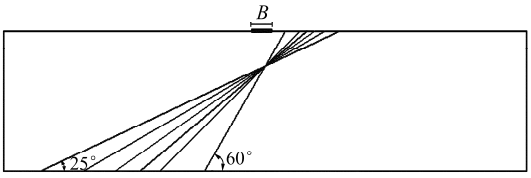

Fig.15 The locations of the assumed joints.

Figure 16 displays the plastic zones near the rock foundation under the limit state when the inclination of the joint is 40°. Figure 17 shows the displacement vector distribution.

Fig.16 Plastic zones near the rock foundation under the limit state.

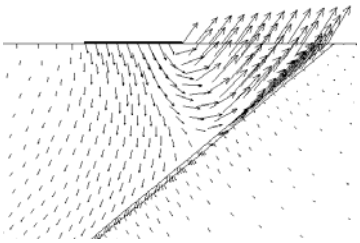

Fig.17 Displacement vector distribution.

The finite element calculation results for the ultimate bearing capacity of a jointed rock foundation with different joint inclinations are listed in Table 12.

Table 12 Calculation results of ultimate bearing capacity of a jointed rock foundation with different joint inclinations.

Joint inclination angle (°)	Calculated bearing capacity (MPa)
25	32.70
30	18.14
35	8.94
40	8.50
45	11.38
60	38.09

For a homogeneous rock foundation, its bearing capacity is 77.75 MPa [21]. As shown in Table 12, because the rock foundation has a joint, the ultimate bearing capacity is controlled by that joint. The change of ultimate bearing capacity of the jointed rock foundation is nonlinear with the joint inclination. As the joint inclination increases, the foundation's ultimate bearing capacity reduces to its minimum and then increases. Therefore, it can be deduced when the joint inclination is less or greater than a certain value, and the existence of the joint has no obvious effects on the ultimate bearing capacity of the rock foundation.

4.4 Numerical analysis of the plate loading test

The plate loading test is the most important method used to acquire the bearing capacity of foundations. It is widely used in confirming the results of foundation treatments. However, there are also shortcomings associated with this method. The shortcomings include size effect, and high economic costs, and consumption of time. We use the finite element limit analysis method by step loading to analyze the plate loading test process and to obtain the bearing capacity of the foundation.

The relevant shear strength parameters include the cohesion c and internal friction angle φ, which can be obtained by in-situ shear tests, laboratory-based shear tests, or laboratory-based triaxial shear tests. A *p*-*s* (load-settlement) relationship of a foundation from the testing is shown in Fig.18 [24]. The *p*-*s* curve is close to a straight line at pressures below 380 kPa. When the pressure rises to 380 kPa, a turning point appears and the curve increases more rapidly with pressure. When the pressure reaches 1.06 MPa, the soil around the support plate heaves upward, indicating foundation failure. According to the building codes, the bearing capacity is set as 960 kPa.

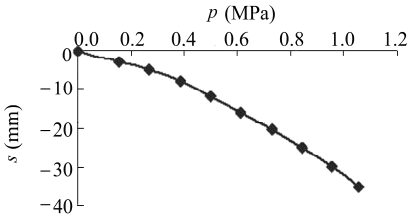

Fig.18 *p*-*s* relation of plate loading test [24].

The mechanical parameters for the foundation are as follows: $\gamma = 22$ kN/m^3, $c = 32.5$ kPa, $\varphi = 30.2°$, Young's modulus E = 17 MPa and Poisson's ratio $\mu = 0.27$. The numerical simulation of the plate loading test is carried out by a step-loading FEM. The finite element model and its meshing are shown in Fig.19. The loading process of the plate loading test is shown in Table 13. The

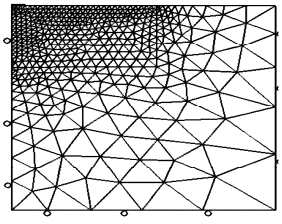

Fig.19 Finite element model and meshing.

Table 13 The step-loading process.

Step-loading No.	Loads (MPa)	Step-loading No.	Loads (MPa)
1	0.15	7	0.11
2	0.12	8	0.12
3	0.11	9	0.10
4	0.12	10	0.07
5	0.11	11	0.01
6	0.12	12	0.01

foundation's bearing capacity is known as 1.14 MPa.

The *p*-*s* curves obtained by the finite element calculation and the plate loading test (Fig.20) indicate good agreement between the FEM calculation results and the measured results.

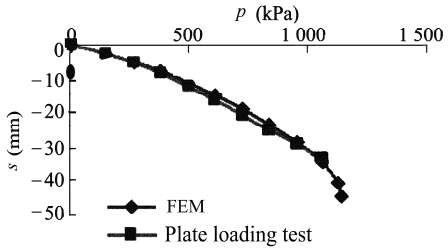

Fig.20 The *p*-*s* relation curves of obtained by FEM and plate loading test.

5 Conclusions

(1) The strength reduction FEM can take pile-soil interactions into consideration, so as to make the analysis technique more reasonable for practical applications. It can be used to determine reasonable pile lengths and make designs safe and economical.

(2) The factor of safety of reservoir banks obtained from the empirical generalization of the phreatic surface is greater than that determined numerically. To put this in context, if for example the slope stability in the Three Gorges reservoir area was analyzed through empirical generalization, the factor of safety would be exaggerated and engineering design could be unsafe.

(3) The step-loading FEM is a useful analysis tool for foundation engineering. Useful results, including the bearing capacity of foundations, load-settlement curves for foundations, and the foundation failure mechanisms, have been readily obtained.

References

[1] Zienkiewicz O C, Humpheson C, Lewis R W. Associated and non-associated visco-plasticity in soil mechanics. Geotechnique, 1975, 25 (4): 671–689.

[2] Matsui T, San K C. Finite element slope stability analysis by shear strength reduction technique. Soils and Foundations, 1992, 32 (1): 59–70.

[3] Griffiths D V, Lane P A. Slope stability analysis by finite elements. Geotechnique, 1999, 49 (3): 387–403.

[4] Lane P A, Griffiths D V. Assessment of stability of slope under drawdown conditions. Journal of Geotechnical and Geoenvironmental Engineering, ASCE, 2000, 126 (5): 443–450.

[5] Smith I M, Griffiths D V. Programming the finite element method. 3rd ed. New York: John Wiley and Sons Inc., 1998.

[6] Dawson E M, Roth W H, Drescher A. Slope stability analysis by strength reduction. Geotechnique, 1999, 49 (6):835–840.

[7] Song Erxiang. Finite element analysis of safety factor. Chinese Journal of Geotechnical Engineering, 1997, 19 (2): 1–7 (in Chinese).

[8] Zheng Yingren, Shen Zhujiang, Gong Xiaonan. Generalized plastic mechanics—the principles of geotechnical plastic mechanics. Beijing: China Architecture and Building Press, 2002.

[9] Lian Zhenying, Han Guocheng, Kong Xianjing. Stability analysis of excavation by strength reduction FEM. Chinese Journal of Geotechnical Engineering, 2001, 23 (4): 407–411 (in Chinese).

[10] Zheng Hong, Li Chunguang, Ge Xiurun. Finite element method for solving the factor of safety. Chinese Journal of Geotechnical Engineering, 2002, 24 (5): 626–628 (in Chinese).

[11] Luan Maotian, Wu Yajun, Nian Tingkai. A criterion for evaluating slope stability based on development of plastic zone by shear strength reduction FEM. Journal of Disaster Prevention and Mitigation Engineering, 2003, 23 (3): 1–8 (in Chinese).

[12] Zhou Cuiying, Liu Zuoqiu, Dong Liguo. Large deformation FEM analysis of slopes failure. Rock and Soil Mechanics, 2003, 24 (4): 644–647 (in Chinese).

[13] Zhao Shangyi, Zheng Yingren, Deng Weidong. Stability analysis of rock slope by strength reduction FEM. Chinese Journal of Rock Mechanics and Engineering, 2003, 22 (2): 254–260 (in Chinese).

[14] Zheng Yingren, Zhao Shangyi, Deng Weidong. Numerical simulation on failure mechanism of rock slope by strength reduction FEM. Chinese Journal of Rock Mechanics and Engineering, 2003, 22 (12): 943–952 (in Chinese).

[15] Zheng Yingren, Zhao Shangyi. Application of strength reduction FEM in soil and rock slope. Chinese Journal of Rock Mechanics and Engineering, 2004, 23 (19): 3 381–3 388 (in Chinese).

[16] Zheng Yingren, Tang Xiaosong. Stability analysis of slopes under drawdown condition of reservoirs. Chinese Journal of Geotechnical Engineering, 2007, 29 (8): 1 115–1 121 (in Chinese).

[17] Tang Xiaosong, Zheng Yingren. Effect of excess pore water pressure on stability of slopes under drawdown condition. Hydro-science and Engineering, 2007, (1): 1–6 (in Chinese).

[18] Tang Xiaosong, Zheng Yingren. The stability analysis of slope under reservoir drawdown condition. Chinese Journal of Geotechnical Engineering, 2007, 27 (8):1 115–1 121 (in Chinese).

[19] Deng Chujian, Kong Weixue, Zheng Yingren. Analysis of ultimate bearing capacity of foundations by elastoplastic FEM through step loading. Rock and Soil Mechanics, 2005, 26 (3): 500–504 (in Chinese).

[20] Kong Weixue, Zheng Yingren, Zhao Shangyi. Finite element analysis for the bearing capacity of foundations and its application in bridge engineering. China Civil Engineering Journal, 2005, 38 (4): 95–100 (in Chinese).

[21] Deng Chujian, Kong Weixue, Zheng Yingren. Analysis of the ultimate bearing capacity of jointed rock foundation by FEM. Industrial Construction, 2005, 35 (12): 51–54 (in Chinese).

[22] Zhou Dongjiu. Study on theoretical formula and safety coefficient of foundation permitting bearing capacity. Communications Standardization, 2003, 8 (3): 31–35 (in Chinese).

[23] Qian Jiahuan, Yin Zongze. Geotechnical principle and calculation. 2nd ed. Beiing: China Water Power Press, 2000 (in Chinese).

[24] Deng Chujian, Tang Xiaosong, Zheng Yingren. Numerical analysis of the plate loading test. Rock and Soil Mechanics, 2007, 28 (Supp.1): 249–253 (in Chinese).